Letter

Anomalous linear and quadratic nodeless surface Dirac cones in three-dimensional Dirac semimetals

Dongling Liu,[*] Xiao-Jiao Wang,[*] Yijie Mo, and Zhongbo Yan[†]
Guangdong Provincial Key Laboratory of Magnetoelectric Physics and Devices, State Key Laboratory of Optoelectronic Materials and Technologies, and School of Physics, Sun Yat-sen University, Guangzhou 510275, China

(Received 1 October 2023; accepted 18 January 2024; published 5 February 2024)

Surface Dirac cones in three-dimensional topological insulators have generated tremendous and enduring interest for almost two decades owing to hosting a multitude of exotic properties. In this work, we unveil the existence of two types of anomalous surface Dirac cones in three-dimensional Dirac semimetals. These surface Dirac cones are located at the surfaces perpendicular to the rotation symmetry axis and are found to display a number of features remarkably different from that in topological insulators. The most prominent one is the absence of a singular Dirac node. In addition, the spin textures of these nodeless surface Dirac cones are found to exhibit a unique two-phase-angle dependence, leading to the presence of two different winding numbers in the orbital-resolved spin textures, which is rather different from the well-known spin-momentum locking in topological insulators. Despite the absence of a Dirac node, we find that the two types of surface Dirac cones are also characterized by quantized π Berry phases, even though one of them takes a quadratic dispersion. In the presence of time-reversal-symmetry-breaking fields, we find that the responses of the surface and bulk Dirac cones display an interesting bulk-surface correspondence. The uncovering of these nodeless surface Dirac cones broadens our understanding of the topological surface states and bulk-boundary correspondence in Dirac semimetals and also lays down the basis for studying unconventional Dirac physics.

DOI: 10.1103/PhysRevB.109.L081401

Since the rise of graphene and topological insulators (TIs), the exploration of Dirac-cone band structures has continued to be at the frontier of a number of disciplines [1–13]. The great interest in Dirac-cone band structures lies in many aspects, such as their relativistic linear dispersions [14], their fundamental connection with topology [15–17], and being the sources of a diversity of unconventional responses [18–25]. The Dirac cones can be roughly classified into two classes, gapped or gapless, with the former (latter) effectively described by a massive (massless) Dirac Hamiltonian [26,27]. A fundamental difference between them is that the gapless Dirac cones carry a symmetry-protected band degeneracy (known as Dirac node or point) that acts as a topological charge. The discovery of an odd number of two-dimensional (2D) gapless Dirac cone on the surface of a 3D strong TI [28–32] has attracted particular interest since it not only provides an exception to the fermion-doubling problem [33–35], but also realizes a class of unconventional metals with many intriguing properties. Notable properties associated with a gapless surface Dirac cone (SDC) include the quantized π Berry phase that can lead to weak antilocalization in transport [36,37] and the spin-momentum-locking Fermi surface [38,39] that can create non-Abliean Majorana zero modes when superconductivity is brought in [40–42]. Moreover, when the gapless SDC is gapped by certain time-reversal symmetry (TRS) breaking field, half-integer quantum Hall effects as well as topological electromagnetic effects can be observed [43–46].

TIs build a common picture through the bulk-boundary correspondence that the 2D gapless SDCs are decedent from the 3D gapped Dirac cones in the bulk [47,48]. However, this does not mean that gapless SDCs can only appear in TIs. As an intermediate phase between TIs and normal insulators, 3D Dirac semimetals (DSMs) with band-inverted structure and rotation symmetry in fact can also support an odd number of 2D gapless Dirac cones on a given surface. This fact was first noticed when Kargarian *et al.* revealed that the Fermi arcs in DSMs could deform into Fermi loops [49], which implies the possibility of the existence of SDCs in DSMs. Later Yan *et al.* analytically derived the low-energy Hamiltonian describing the surface states and showed how the gapless SDCs arise [50]. All these studies, however, are restricted to the side surfaces parallel to the rotation axis where the bulk Dirac nodes are located, owing to the primary interest in Fermi arcs and the fact that Fermi arcs only exist on the surfaces where the projections of the bulk Dirac nodes do not overlap [51].

Recently, a remarkable experiment reported the observation of 2D gapless SDCs in some iron-based superconducting compounds with 3D bulk Dirac nodes protected by C_{4z} rotation symmetry [52]. Notably, the 2D gapless Dirac cones are located on the surface where the projections of the bulk Dirac nodes overlap, revealing that the largely overlooked top and bottom surfaces perpendicular to the rotation axis also carry interesting topological surface states in DSMs. Inspired by this experiment, we consider two representative types of 3D

[*]These authors contributed equally to this work.
[†]yanzhb5@mail.sysu.edu.cn

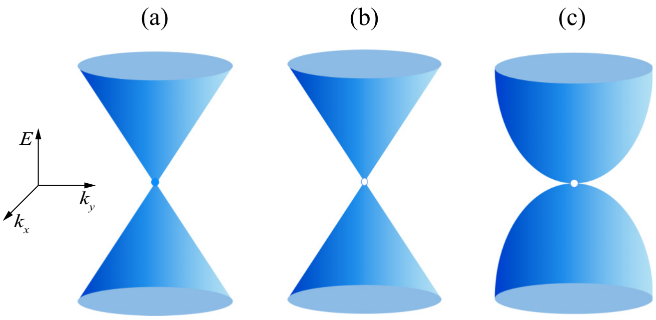

FIG. 1. Schematic diagrams of three types of gapless SDCs. (a) Linear SDC in TIs; the Dirac node (a Kramers degeneracy) denoted by a solid dot is enforced by TRS. Panels (b) and (c) are respectively the linear and quadratic nodeless SDCs in the opposite-parity and same-parity DSMs. The open circles in (b) and (c) represent the absence of Dirac node.

DSMs protected by C_{4z} rotation symmetry and explore the topological surface states on the top and bottom surfaces. Remarkably, we find that the gapless Dirac cones found on these surfaces display a number of features sharply distinct from the SDCs in TIs. The most evident difference is the absence of Dirac node in them, as illustrated in Fig. 1. The spin textures of these nodeless SDCs are found to have a unique two-phase-angle dependence enforced by a subchiral symmetry, rather different from the one-phase-angle dependence exhibited in TIs. Furthermore, despite the absence of Dirac node, we find that the two types of SDCs are also characterized by quantized π Berry phases, even though one of them has a quadratic dispersion. In the presence of TRS-breaking fields, we find that the responses of the surface and bulk Dirac cones display an interesting bulk-surface correspondence.

Linear nodeless SDCs in the opposite-parity DSM. DSMs are materials whose conduction and valence bands cross at some isolated points (Dirac nodes) in the Brillouin zone [53–59]. Depending on whether the band crossings occur between bands with opposite parity or same parity, DSMs can be roughly divided into two classes [60]. For the convenience of discussion, we dub the class involving bands with opposite (same) parity as opposite-parity (same-parity) DSMs.

Let us first consider the opposite-parity DSM. Focusing on a cubic-lattice realization, the minimal model is given by [55,61]

$$\begin{aligned}\mathcal{H}(\boldsymbol{k}) = &(m - t\ \cos k_x - t\ \cos k_y - t_z \cos k_z)\sigma_z s_0\\ &+\lambda(\sin k_x\sigma_x s_z - \sin k_y\sigma_y s_0)\\ &+\eta_1(\boldsymbol{k}_s)\sin k_z\sigma_x s_x + \eta_2(\boldsymbol{k}_s)\sin k_z\sigma_x s_y,\end{aligned} \tag{1}$$

where $\boldsymbol{k}_s = (k_x, k_y)$ denotes the xy-plane momentum, $\eta_1(\boldsymbol{k}_s) = \eta_1(\cos k_x - \cos k_y)$, $\eta_2(\boldsymbol{k}_s) = \eta_2 \sin k_x \sin k_y$, σ_i and s_i are Pauli matrices in orbital and spin space, and σ_0 and s_0 are the corresponding identity matrices. For notational simplicity, the lattice constants are set to unity throughout. Without loss of generality, below we consider all parameters in Eq. (1) to be positive and $|m - 2t| < t_z < m$. Accordingly, a band inversion occurs at the time-reversal invariant momentum $\boldsymbol{\Gamma} = (0, 0, 0)$ and there are two Dirac nodes located at $\boldsymbol{k}_{D,\pm} = \pm(0, 0, k_D)$ with $k_D = \arccos(m - 2t)/t_z$.

It is noteworthy that the existence and the locations of the bulk Dirac nodes do not depend on the two η terms. However, as we shall show below, the η terms have rather remarkable effects on the topological surface states.

When η_1 and η_2 vanish, the Hamiltonian (1) at a given k_z is characterized by a Z_2 invariant [5] and describes a 2D TI for $|k_z| < |\boldsymbol{k}_D|$ and a normal insulator for $|k_z| > |\boldsymbol{k}_D|$. For this situation, the DSM can be regarded as a stacking of 2D TIs in the z direction. Accordingly, the surface states only exist on the side surfaces and the isoenergy contours of these surface states form the so-called Fermi arcs. Once η_1 and η_2 become finite, the dispersions of the surface states on the side surfaces change dramatically [49,50,62–64], leading to the change of the Fermi-arc connectivity and the rise of SDCs that can have nontrivial interplay with superconductivity [65–67]. Furthermore, it has been recognized that the η terms can also give rise to gapless hinge states [68], a hallmark of second-order topology. These findings have one after another deepened our understanding on the bulk-boundary correspondence of DSMs. Now we show that our understanding remains incomplete.

To intuitively show that 2D gapless Dirac cones also exist on the top and bottom surfaces, we first introduce a set of momentum-dependent Pauli matrices, namely,

$$\begin{aligned}\tilde{s}_x &= \cos\theta_{\boldsymbol{k}_s} s_x + \sin\theta_{\boldsymbol{k}_s} s_y,\\ \tilde{s}_y &= -\sin\theta_{\boldsymbol{k}_s} s_x + \cos\theta_{\boldsymbol{k}_s} s_y,\\ \tilde{s}_z &= s_z,\end{aligned} \tag{2}$$

where $\theta_{\boldsymbol{k}_s} = \arg[\eta_1(\boldsymbol{k}_s) + i\eta_2(\boldsymbol{k}_s)]$. In this work, two phase angles will be involved—one is $\theta_{\boldsymbol{k}_s}$ and the other is $\phi_{\boldsymbol{k}_s} = \arg(\sin k_x + i\ \sin k_y)$. When considering the continuum counterpart of the lattice Hamiltonian, these two phase angles are implicitly assumed to take the corresponding continuum forms [e.g., $\phi_{\boldsymbol{k}_s} = \arg(k_x + ik_y)$].

It is easy to verify that this set of Pauli matrices also satisfies $[\tilde{s}_i, \tilde{s}_j] = 2i\epsilon_{ijk}\tilde{s}_k$ and $\{\tilde{s}_i, \tilde{s}_j\} = 2\delta_{ij}s_0$ for $i, j \in \{x, y, z\}$. Using them, the Hamiltonian can be rewritten as

$$\begin{aligned}\mathcal{H}(\boldsymbol{k}) = &(m - t\ \cos k_x - t\ \cos k_y - t_z \cos k_z)\sigma_z s_0\\ &+ \lambda(\sin k_x\sigma_x\tilde{s}_z - \sin k_y\sigma_y s_0)\\ &+ \eta(\boldsymbol{k}_s)\sin k_z\sigma_x\tilde{s}_x,\end{aligned} \tag{3}$$

where $\eta(\boldsymbol{k}_s) = \sqrt{\eta_1^2(\boldsymbol{k}_s) + \eta_2^2(\boldsymbol{k}_s)}$. The above form resembles the minimal model for 3D TIs [47], suggesting the existence of gapless Dirac cones on the z-normal surfaces if $\eta(\boldsymbol{k}_s)$ is nonzero. In this form, it is also easy to see that there exists a unitary operator anticommuting with the Hamiltonian, i.e., $\{\mathcal{C}, \mathcal{H}\} = 0$, with $\mathcal{C} = \sigma_x\tilde{s}_y$. Conventionally, such an anticommutation relation suggests that the Hamiltonian has chiral symmetry. However, this is not the case here, simply because the operator $\mathcal{C}$ is not a constant operator but depends on partial components of the momentum vector. Such an algebraic property was recently discussed and dubbed subchiral symmetry in Ref. [69]. An important conclusion from Ref. [69] is that the subchiral symmetry operator itself admits topological characterization and its topological property will impart into the spin texture of the topological boundary states. Apparently, here $\tilde{s}_y$ displays a nontrivial winding as $\boldsymbol{k}_s$ goes around the origin once, indicating the nontrivialness of the subchiral symmetry operator.

Now let us proceed to derive the low-energy Hamiltonians describing the gapless Dirac cones on the z-normal surfaces. The methods are well developed [26]. As usual, the first step is to do a low-energy expansion of the bulk Hamiltonian around the band-inversion momentum and decompose the Hamiltonian into two parts [70], i.e., $\mathcal{H} = \mathcal{H}_0 + \mathcal{H}_1$, with (see more details in the Supplemental Material [71])

$$\mathcal{H}_0(\boldsymbol{k}) = \left[M(\boldsymbol{k}_s) + \frac{t_z}{2}k_z^2\right]\sigma_z s_0 + \gamma(\boldsymbol{k}_s)k_z\sigma_x\tilde{s}_x,$$
$$\mathcal{H}_1(\boldsymbol{k}) = \lambda(k_x\sigma_x\tilde{s}_z - k_y\sigma_y s_0), \tag{4}$$

where $M(\boldsymbol{k}_s) = m - 2t - t_z + t(k_x^2 + k_y^2)/2$ and $\gamma(\boldsymbol{k}_s) = \frac{1}{2}\sqrt{\eta_1^2(k_x^2 - k_y^2)^2 + 4\eta_2^2 k_x^2 k_y^2}$. Considering a half-infinity system occupying $z \geqslant 0$ ($z \leqslant 0$), replacing $k_z \to -i\partial_z$, and solving the eigenvalue equation $\mathcal{H}_0(\boldsymbol{k}_s, -i\partial_z)\psi_\alpha(x, y, z) = 0$ under the boundary conditions $\psi_\alpha(z = 0) = 0$ and $\psi_\alpha(z \to \infty) = 0$ [$\psi_\alpha(z \to -\infty) = 0$], one will obtain two solutions corresponding to the zero-energy boundary states at the bottom (top) surface. Their explicit forms read [72]

$$\psi_\alpha^a(x, y, z) = \mathcal{N}\ \sin(\kappa_1 z)e^{-\kappa_2|z|}e^{i(k_x x + k_y y)}\chi_\alpha^a, \tag{5}$$

where the superscript $a = \{t, b\}$ labels the top and bottom surfaces, $\kappa_1 = \sqrt{-2t_z M(\boldsymbol{k}_s) - \gamma^2(\boldsymbol{k}_s)}/t_z$, $\kappa_2 = \gamma(\boldsymbol{k}_s)/t_z$, $\mathcal{N}$ is a normalization constant, χ_α^t satisfy $\sigma_y\tilde{s}_x\chi_\alpha^t = \chi_\alpha^t$, and χ_α^b satisfy $\sigma_y\tilde{s}_x\chi_\alpha^b = -\chi_\alpha^b$. The normalizability of the wave functions determines the region hosting boundary states, which turns out to be the region bound by the projection of the band-inversion surface, i.e., $M(\boldsymbol{k}_s) < 0$. Noteworthily, the point $\boldsymbol{k}_s = \boldsymbol{0}$, however, needs to be excluded since $\gamma(\boldsymbol{k}_s)$ vanishes at this point. This result is consistent with the fact that the effective 1D Hamiltonian $\mathcal{H}(0, 0, k_z)$ is gapless and the projections of the two bulk Dirac nodes are exactly located at this surface time-reversal invariant momentum [55].

The low-energy Hamiltonians for the top and bottom surfaces are obtained by projecting $\mathcal{H}_1(\boldsymbol{k})$ onto the Hilbert space spanned by the corresponding two zero-energy eigenstates. Since $[\sigma_y\tilde{s}_x, \mathcal{C}] = 0$, we can choose $\chi_\alpha^{t/b}$ to be the eigenstates of the subchiral symmetry operator. Without loss of generality, we choose $\chi_\pm^t = (|\sigma_y = 1, \tilde{s}_x = 1\rangle \pm |\sigma_y = -1, \tilde{s}_x = -1\rangle)/\sqrt{2}$ and $\chi_\pm^b = (|\sigma_y = 1, \tilde{s}_x = -1\rangle \mp |\sigma_y = -1, \tilde{s}_x = 1\rangle)/\sqrt{2}$, so that $\mathcal{C}\chi_\pm^{t/b} = \pm\chi_\pm^{t/b}$. Here $|\sigma_y = \pm 1, \tilde{s}_x = \pm 1\rangle$ stands for $|\sigma_y = \pm 1\rangle \otimes |\tilde{s}_x = \pm 1\rangle$, with $\sigma_y|\sigma_y = \pm 1\rangle = \pm|\sigma_y = \pm 1\rangle$ and $\tilde{s}_x|\tilde{s}_x = \pm 1\rangle = \pm|\tilde{s}_x = \pm 1\rangle$. Accordingly, in the basis of $(\psi_-^t, \psi_+^t)^T$ or $(\psi_+^b, \psi_-^b)^T$, the low-energy surface Hamiltonians are found to take the off-diagonal form

$$\mathcal{H}_{t/b}(\boldsymbol{k}_s) = \lambda(k_x\rho_y - k_y\rho_x), \tag{6}$$

where ρ_i denote Pauli matrices acting on the two eigenstates of the subchiral symmetry operator. Apparently, the surface Hamiltonians take the exactly same form as in TIs [47]. However, here the linearly dispersive SDCs have two fundamental differences. First, as discussed above, surface states are absent at $\boldsymbol{k}_s = \boldsymbol{0}$. This fact indicates the absence of Dirac node in this class of SDCs. Second, here the basis functions are the eigenstates of the subchiral symmetry operator, which themselves carry nontrivial topological properties as the subchiral symmetry operator displays a nontrivial winding with respect to the momentum. As will be shown below, this property has nontrivial effects on the spin texture and Berry phase.

To determine the spin texture and Berry phase, we need to first determine the spinor part of the wave functions for the SDCs. To be specific, let us focus on the upper band of the top-surface Dirac cone for a detailed discussion (the spin texture for the bottom-surface Dirac cone is just the opposite and the Berry phase is the same). According to the form of $\mathcal{H}_t$ in Eq. (6), it is easy to find that the eigenstate for the upper band is $(1, ie^{i\phi_{\boldsymbol{k}_s}})^T/\sqrt{2}$. By further taking into account the nontrivial basis functions, the corresponding spinor takes the form

$$|u(\boldsymbol{k}_s)\rangle = \frac{1}{\sqrt{2}}(\chi_-^t + ie^{i\phi_{\boldsymbol{k}_s}}\chi_+^t). \tag{7}$$

Because the spin and orbital are entangled by spin-orbit coupling, we consider the orbital-resolved spin texture [73–75], which are given by $\bar{s}_i^{(o_\pm)}(\boldsymbol{k}_s) = \langle u(\boldsymbol{k}_s)|(\sigma_0 \pm \sigma_z)s_i|u(\boldsymbol{k}_s)\rangle/2$, where the two superscripts o_+ and o_- label the two orbitals (here we ignore the constant factor $\hbar/2$ connecting the Pauli matrices to the spin operators). A straightforward calculation obtains

$$\bar{s}_x^{(o_\pm)}(\boldsymbol{k}_s) = \pm[\sin(\theta_{\boldsymbol{k}_s} \mp \phi_{\boldsymbol{k}_s})]/2,$$
$$\bar{s}_y^{(o_\pm)}(\boldsymbol{k}_s) = \mp[\cos(\theta_{\boldsymbol{k}_s} \mp \phi_{\boldsymbol{k}_s})]/2,$$
$$\bar{s}_z^{(o_\pm)}(\boldsymbol{k}_s) = 0. \tag{8}$$

The spin polarizations are aligned in the surface plane. This is similar to the spin textures of the SDCs in TIs. However, here a striking difference is that the spin textures depend on two phase angles rather than one as in TIs [75]. Particularly, the angle $\theta_{\boldsymbol{k}_s}$ originates from the subchiral symmetry and will change 4π when the polar angle of the surface momentum changes 2π. Due to the unique two-phase-angle dependence, the two orbital-resolved spin textures display a remarkable property, namely, their spin polarizations wind one and three times, respectively, when $\boldsymbol{k}_s$ winds the origin once, as shown in Figs. 2(a)–2(c). This is rather different from the TI for which only one time of winding will exhibit [6,7].

Also based on $|u(\boldsymbol{k}_s)\rangle$, the Berry connection is given by [76]

$$A_\alpha(\boldsymbol{k}_s) = -i\langle u(\boldsymbol{k}_s)|\partial_{k_\alpha}u(\boldsymbol{k}_s)\rangle = \tfrac{1}{2}\partial_{k_\alpha}(\theta_{\boldsymbol{k}_s} + \phi_{\boldsymbol{k}_s}), \tag{9}$$

where $\alpha = \{x, y\}$. Since $\theta_{\boldsymbol{k}_s}$ will wind 4π and $\phi_{\boldsymbol{k}_s}$ will wind 2π when $\boldsymbol{k}_s$ winds 2π, it indicates that one particle will accumulate a π (mod 2π) Berry phase when it goes around the surface Fermi loop once. This important result indicates that the quantized π Berry phase remains intact even though the singular Dirac node is absent in the SDCs.

Quadratic nodeless SDCs in the same-parity DSM. Let us move our attention to the same-parity DSM. Also focusing on a cubic-lattice realization, the minimal model is given by [61]

$$\mathcal{H}(\boldsymbol{k}) = (m - t\ \cos k_x - t\ \cos k_y - t_z\cos k_z)\sigma_z s_0$$
$$+\lambda\ \sin k_z(\sin k_x\sigma_x s_0 - \sin k_y\sigma_y s_z)$$
$$+\eta_1(\boldsymbol{k}_s)\sigma_y s_x + \eta_2(\boldsymbol{k}_s)\sigma_y s_y. \tag{10}$$

Without loss of generality, below we again consider all parameters to be positive and $|m - 2t| < t_z < m$ so that the two bulk

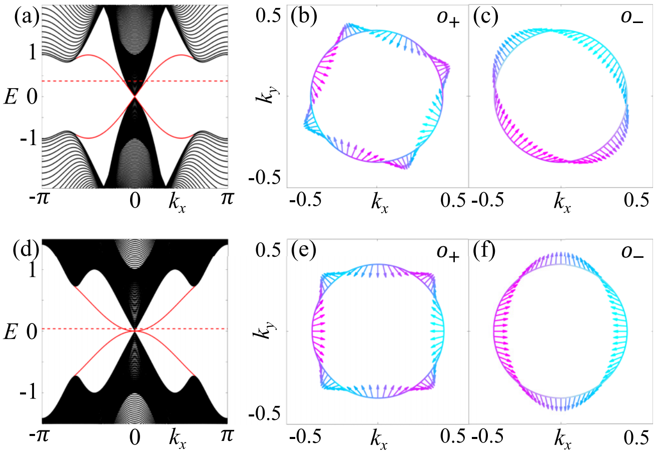

FIG. 2. Energy spectra at $k_y = 0$ for a sample with open (periodic) boundary conditions in the z (x and y) direction and spin textures of the top-surface Dirac cones. The solid red lines in (a) and (d) show the existence of linear and quadratic SDCs in the opposite-parity and same-parity DSMs, respectively. The orbital-resolved spin textures in (b) and (c) [(e) and (f)] are plotted on the isoenergy contour of the SDC illustrated by the red dashed line corresponding to $E = 0.375$ (0.038) in (a) [(d)]. Common parameters are $m = 3$, $t = t_z = 2$, and $\lambda = 1$. $\eta_1 = \eta_2 = 5$ in (a)–(c) and $\eta_1 = \eta_2 = 0.5$ in (d)–(f).

Dirac nodes are also located at $\boldsymbol{k}_{D,\pm}$. Similar to the first model, this model also supports interesting gapless topological states on the side surfaces and hinges [68]. However, much less is known about the top and bottom surfaces. Below we explore the surface states on these two surfaces.

The first thing to note is that the Hamiltonian (10) also has a subchiral symmetry, with the symmetry operator given by

$$\tilde{C} = \sin\phi_{\boldsymbol{k}_s}\sigma_x s_0 + \cos\phi_{\boldsymbol{k}_s}\sigma_y s_z. \tag{11}$$

Also using the continuum-model approach, we find that the wave functions of surface states on the top and bottom surfaces are given by

$$\tilde{\psi}^a_\alpha(x, y, z) = \tilde{\mathcal{N}}\,\sin(\tilde{\kappa}_1 z)e^{-\tilde{\kappa}_2|z|}e^{i(k_x x + k_y y)}\tilde{\chi}^a_\alpha, \tag{12}$$

where $\tilde{\kappa}_1 = \sqrt{-2t_z M(\boldsymbol{k}_s) - \lambda^2\boldsymbol{k}_s^2}/t_z$, $\tilde{\kappa}_2 = \lambda|\boldsymbol{k}_s|/t_z$, and $\tilde{\chi}^a_\alpha$ satisfy $\tilde{C}\tilde{\chi}^a_\alpha = \alpha\tilde{\chi}^a_\alpha$ with $\alpha = \pm$. The normalizability of the wave functions also suggests that the region hosting surface states corresponds to $M(\boldsymbol{k}_s) < 0$ but with the point $\boldsymbol{k}_s = \boldsymbol{0}$ excluded. Without loss of generality, we choose $\tilde{\chi}^t_\pm = |\sigma_\pm = \pm 1, s_z = \pm 1\rangle$ and $\tilde{\chi}^b_\mp = |\sigma_\pm = \mp 1, s_z = \pm 1\rangle$, where $\sigma_\pm = \sin\phi_{\boldsymbol{k}_s}\sigma_x \pm \cos\phi_{\boldsymbol{k}_s}\sigma_y$. In the basis of $(\tilde{\psi}^t_+, \tilde{\psi}^t_-)^T$ or $(\tilde{\psi}^b_-, \tilde{\psi}^b_+)^T$, the low-energy surface Hamiltonians are found to take the off-diagonal form

$$\mathcal{H}_{t/b}(\boldsymbol{k}_s) = \pm\begin{pmatrix} 0 & \eta_-(\boldsymbol{k}_s)e^{i\phi_{\boldsymbol{k}_s}} \\ \eta_+(\boldsymbol{k}_s)e^{-i\phi_{\boldsymbol{k}_s}} & 0 \end{pmatrix}, \tag{13}$$

where + (−) refers to the top (bottom) surface and $\eta_\pm(\boldsymbol{k}_s) = -\frac{\eta_1}{2}(k_x^2 - k_y^2) \pm i\eta_2 k_x k_y$. It is easy to see that the energy dispersions of the surface Hamiltonian are given by $E_\pm(\boldsymbol{k}_s) = \pm\sqrt{\eta_+(\boldsymbol{k}_s)\eta_-(\boldsymbol{k}_s)}$, which are quadratic rather than linear, as shown in Fig. 2(d). It is worth emphasizing that the Dirac node is also absent for this class of quadratic SDCs.

Again let us focus on the upper band of the top-surface Dirac cone for a discussion of its spin texture and Berry phase. The corresponding spinor part of the wave function is found to take the form

$$|\tilde{u}(\boldsymbol{k}_s)\rangle = \frac{1}{\sqrt{2}}\left(\tilde{\chi}^t_+ + e^{i(\theta_{\boldsymbol{k}_s} - \phi_{\boldsymbol{k}_s})}\tilde{\chi}^t_-\right). \tag{14}$$

Based on $|\tilde{u}(\boldsymbol{k}_s)\rangle$, one finds

$$\begin{aligned} \bar{s}_x^{(o_\pm)}(\boldsymbol{k}_s) &= [\cos(\theta_{\boldsymbol{k}_s} \mp \phi_{\boldsymbol{k}_s})]/2, \\ \bar{s}_y^{(o_\pm)}(\boldsymbol{k}_s) &= [\sin(\theta_{\boldsymbol{k}_s} \mp \phi_{\boldsymbol{k}_s})]/2, \\ \bar{s}_z^{(o_\pm)}(\boldsymbol{k}_s) &= 0. \end{aligned} \tag{15}$$

The two orbital-resolved spin textures also depend on two phase angles and display different windings, as shown in Figs. 2(e) and 2(f). The Berry connection is given by

$$A_\alpha(\boldsymbol{k}_s) = -i\langle\tilde{u}(\boldsymbol{k}_s)|\partial_{k_\alpha}\tilde{u}(\boldsymbol{k}_s)\rangle = \tfrac{1}{2}\partial_{k_\alpha}(\theta_{\boldsymbol{k}_s} - \phi_{\boldsymbol{k}_s}). \tag{16}$$

Similarly, this result indicates that the particle will accumulate a π (mod 2π) Berry phase when it goes around the surface Fermi loop once. This is a remarkable result since usually a quadratic cone is accompanied with a zero (mod 2π) Berry phase [77]. From Eq. (16), it is apparent that the π Berry phase is attributed to $\phi_{\boldsymbol{k}_s}$, indicating its origin from the subchiral symmetry rather than the quadratic band structure.

Response to TRS-breaking fields. It is known that the SDCs in TIs are protected by TRS and the lift of TRS can gap the SDCs [43,78]. On the other hand, it is known that TRS-breaking fields will split one bulk Dirac node into two Weyl nodes [9]. Here the SDCs are nodeless and therefore are not protected by TRS. To open a gap to the SDCs, mathematically a Dirac mass term of the form $m_D\rho_z$ is required to enter into the surface Hamiltonian (6) or (13). As the basis functions for the surface Hamiltonians are eigenstates of the subchiral

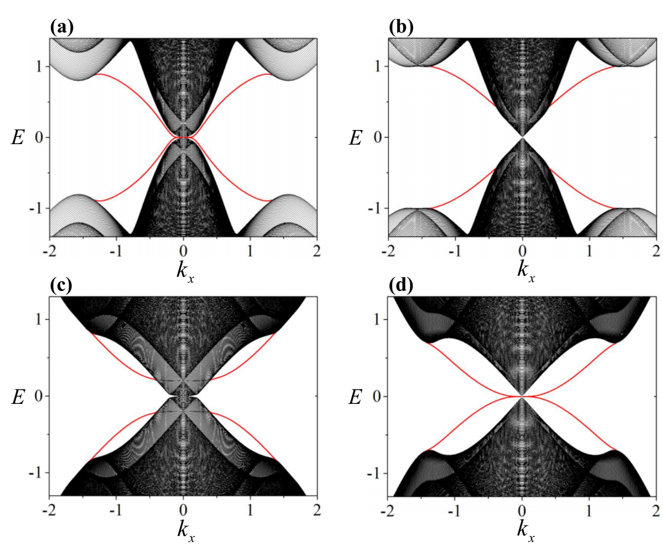

FIG. 3. Energy spectra at $k_y = 0$ for a sample with open boundary conditions only in the z direction (lattice sites $N_z = 400$). Common parameters are $m = 4$, $t = t_z = 2$, and $\lambda = 1$. The values of $(\eta_1, \eta_2, B_1, B_2)$ in (a), (b), (c), and (d) are (5,5,0.2,0), (5,5,0,0.2), (1,1,0.2,0), and (1,1,0,0.2), respectively. Panels (a) and (b) correspond to the opposite-parity DSM and (c) and (d) refer to the same-parity DSM.

symmetry operators, a necessary but not sufficient condition to generate the Dirac mass term is that the TRS-breaking fields must commute with the subchiral symmetry operator. To demonstrate the above arguments, we consider two types of Zeeman splitting fields, i.e., $B_1\sigma_0 s_z$ and $B_2\sigma_z s_z$. For the opposite-parity DSM, $B_1\sigma_0 s_z$ preserves the subchiral symmetry, while $B_2\sigma_z s_z$ does not. The situation is just the opposite for the same-parity DSM. As shown in Fig. 3, the results show that $B_2\sigma_z s_z$ gaps the SDCs in the opposite-parity DSM, while $B_1\sigma_0 s_z$ gaps the SDCs in the same-parity DSM, which is consistent with the above analysis. Interestingly, we note that, no matter whether the SDCs are gapped or not, the surface states are always connected with the bulk nodes, either at $E = 0$ or $\pm B_1$ ($\pm B_2$), which can be viewed as a kind of bulk-surface correspondence. Furthermore, for the gapless cases shown in Figs. 3(a) and 3(d), we note that the Zeeman fields flatten the SDCs, which may have nontrivial interplay with interactions.

Discussions and conclusions. We have unveiled the existence of two types of nodeless SDCs with linear and quadratic dispersion, quantized π Berry phases and unconventional spin textures, expanding our understanding of the topological surface states and bulk-boundary correspondence in DSMs. Our predictions are of general relevance as our theory is based on two generic classes of DSMs. In experiments, the dispersion of the SDCs and the concomitant unconventional spin textures can be directly detected by using spin-resolved and angle-resolved photoemission spectroscopy [39,52,79–83]. To conclude, our work exemplifies that the subchiral symmetry can enrich the properties of the topological boundary states and our findings diversify the types of SDCs with fascinating properties, opening directions for future studies of unconventional Dirac physics.

We would like to thank Z. Wu for helpful discussions and insightful comments. This work is supported by the National Natural Science Foundation of China (Grant No. 12174455), the Natural Science Foundation of Guangdong Province (Grant No. 2021B1515020026), and the Guangdong Basic and Applied Basic Research Foundation (Grant No. 2023B1515040023).

[1] K. S. Novoselov, A. K. Geim, S. V. Morozov, D. Jiang, Y. Zhang, S. V. Dubonos, I. V. Grigorieva, and A. A. Firsov, Electric field effect in atomically thin carbon films, Science **306**, 666 (2004).

[2] C. L. Kane and E. J. Mele, Quantum spin Hall effect in graphene, Phys. Rev. Lett. **95**, 226801 (2005).

[3] C. L. Kane and E. J. Mele, Z_2 topological order and the quantum spin Hall effect, Phys. Rev. Lett. **95**, 146802 (2005).

[4] B. A. Bernevig and S.-C. Zhang, Quantum spin Hall effect, Phys. Rev. Lett. **96**, 106802 (2006).

[5] B. A. Bernevig, T. L. Hughes, and S.-C. Zhang, Quantum spin hall effect and topological phase transition in hgte quantum wells, Science **314**, 1757 (2006).

[6] M. Z. Hasan and C. L. Kane, *Colloquium*: Topological insulators, Rev. Mod. Phys. **82**, 3045 (2010).

[7] X.-L. Qi and S.-C. Zhang, Topological insulators and superconductors, Rev. Mod. Phys. **83**, 1057 (2011).

[8] O. Vafek and A. Vishwanath, Dirac fermions in solids: From high-T_c cuprates and graphene to topological insulators and weyl semimetals, Annu. Rev. Condens. Matter Phys. **5**, 83 (2014).

[9] N. P. Armitage, E. J. Mele, and A. Vishwanath, Weyl and Dirac semimetals in three-dimensional solids, Rev. Mod. Phys. **90**, 015001 (2018).

[10] L. Lu, J. D. Joannopoulos, and M. Soljačić, Topological photonics, Nat. Photon. **8**, 821 (2014).

[11] T. Ozawa, H. M. Price, A. Amo, N. Goldman, M. Hafezi, L. Lu, M. C. Rechtsman, D. Schuster, J. Simon, O. Zilberberg, and I. Carusotto, Topological photonics, Rev. Mod. Phys. **91**, 015006 (2019).

[12] G. Ma, M. Xiao, and C. T. Chan, Topological phases in acoustic and mechanical systems, Nat. Rev. Phys. **1**, 281 (2019).

[13] H. Xue, Y. Yang, and B. Zhang, Topological acoustics, Nat. Rev. Mater. **7**, 974 (2022).

[14] K. S. Novoselov, A. K. Geim, S. V. Morozov, D. Jiang, M. I. Katsnelson, I. V. Grigorieva, S. V. Dubonos, and A. A. Firsov, Two-dimensional gas of massless Dirac fermions in graphene, Nature (London) **438**, 197 (2005).

[15] R. Jackiw and C. Rebbi, Solitons with fermion number 1/2, Phys. Rev. D **13**, 3398 (1976).

[16] S. Ryu, A. P. Schnyder, A. Furusaki, and A. W. W. Ludwig, Topological insulators and superconductors: Tenfold way and dimensional hierarchy, New J. Phys. **12**, 065010 (2010).

[17] C.-K. Chiu, J. C. Y. Teo, A. P. Schnyder, and S. Ryu, Classification of topological quantum matter with symmetries, Rev. Mod. Phys. **88**, 035005 (2016).

[18] P. Cheng, C. Song, T. Zhang, Y. Zhang, Y. Wang, J.-F. Jia, J. Wang, Y. Wang, B.-F. Zhu, X. Chen, X. Ma, K. He, L. Wang, X. Dai, Z. Fang, X. Xie, X.-L. Qi, C.-X. Liu, S.-C. Zhang, and Q.-K. Xue, Landau quantization of topological surface states in Bi_2Se_3, Phys. Rev. Lett. **105**, 076801 (2010).

[19] W.-K. Tse and A. H. MacDonald, Giant magneto-optical kerr effect and universal faraday effect in thin-film topological insulators, Phys. Rev. Lett. **105**, 057401 (2010).

[20] I. Garate and M. Franz, Inverse spin-galvanic effect in the interface between a topological insulator and a ferromagnet, Phys. Rev. Lett. **104**, 146802 (2010).

[21] J. Xiong, S. K. Kushwaha, T. Liang, J. W. Krizan, M. Hirschberger, W. Wang, R. J. Cava, and N. P. Ong, Evidence for the chiral anomaly in the Dirac semimetal Na_3Bi, Science **350**, 413 (2015).

[22] L. Wu, M. Salehi, N. Koirala, J. Moon, S. Oh, and N. P. Armitage, Quantized Faraday and Kerr rotation and axion electrodynamics of a 3D topological insulator, Science **354**, 1124 (2016).

[23] Q. Li, D. E. Kharzeev, C. Zhang, Y. Huang, I. Pletikosić, A. V. Fedorov, R. D. Zhong, J. A. Schneeloch, G. D. Gu, and T. Valla, Chiral magnetic effect in $ZrTe_5$, Nat. Phys. **12**, 550 (2016).

[24] X. Yuan, Z. Yan, C. Song, M. Zhang, Z. Li, C. Zhang, Y. Liu, W. Wang, M. Zhao, Z. Lin, T. Xie, J. Ludwig, Y. Jiang, X. Zhang, C. Shang, Z. Ye, J. Wang, F. Chen, Z. Xia, D. Smirnov *et al.*,

Chiral Landau levels in Weyl semimetal NbAs with multiple topological carriers, Nat. Commun. **9**, 1854 (2018).

[25] X. Yuan, C. Zhang, Y. Zhang, Z. Yan, T. Lyu, M. Zhang, Z. Li, C. Song, M. Zhao, P. Leng, M. Ozerov, X. Chen, N. Wang, Y. Shi, H. Yan, and F. Xiu, The discovery of dynamic chiral anomaly in a Weyl semimetal NbAs, Nat. Commun. **11**, 1259 (2020).

[26] S.-Q. Shen, *Topological Insulators: Dirac Equation in Condensed Matters* (Springer Science & Business Media, New York, 2013), Vol. 174.

[27] B. A. Bernevig and T. L. Hughes, *Topological Insulators and Topological Superconductors* (Princeton University Press, Princeton, NJ, 2013).

[28] Y. Xia, D. Qian, D. Hsieh, L. Wray, A. Pal, H. Lin, A. Bansil, D. Grauer, Y. S. Hor, R. J. Cava, and M. Z. Hasan, Observation of a large-gap topological-insulator class with a single Dirac cone on the surface, Nat. Phys. **5**, 398 (2009).

[29] D. Hsieh, Y. Xia, D. Qian, L. Wray, F. Meier, J. H. Dil, J. Osterwalder, L. Patthey, A. V. Fedorov, H. Lin, A. Bansil, D. Grauer, Y. S. Hor, R. J. Cava, and M. Z. Hasan, Observation of time-reversal-protected single-Dirac-cone topological-insulator states in Bi_2Te_3 and Sb_2Te_3, Phys. Rev. Lett. **103**, 146401 (2009).

[30] Y. L. Chen, J. G. Analytis, J.-H. Chu, Z. K. Liu, S.-K. Mo, X. L. Qi, H. J. Zhang, D. H. Lu, X. Dai, Z. Fang, S. C. Zhang, I. R. Fisher, Z. Hussain, and Z.-X. Shen, Experimental realization of a three-dimensional topological insulator, Bi_2Te_3, Science **325**, 178 (2009).

[31] T. Sato, K. Segawa, H. Guo, K. Sugawara, S. Souma, T. Takahashi, and Y. Ando, Direct evidence for the Dirac-cone topological surface states in the ternary chalcogenide $TlBiSe_2$, Phys. Rev. Lett. **105**, 136802 (2010).

[32] Y. L. Chen, Z. K. Liu, J. G. Analytis, J.-H. Chu, H. J. Zhang, B. H. Yan, S.-K. Mo, R. G. Moore, D. H. Lu, I. R. Fisher, S. C. Zhang, Z. Hussain, and Z.-X. Shen, Single Dirac cone topological surface state and unusual thermoelectric property of compounds from a new topological insulator family, Phys. Rev. Lett. **105**, 266401 (2010).

[33] H. B. Nielsen and M. Ninomiya, A no-go theorem for regularizing chiral fermions, Phys. Lett. B **105**, 219 (1981).

[34] H. B. Nielsen and M. Ninomiya, Absence of neutrinos on a lattice: (I). Proof by homotopy theory, Nucl. Phys. B **185**, 20 (1981).

[35] H. B. Nielsen and M. Ninomiya, Absence of neutrinos on a lattice: (II). Intuitive topological proof, Nucl. Phys. B **193**, 173 (1981).

[36] H.-T. He, G. Wang, T. Zhang, I.-K. Sou, G. K. L. Wong, J.-N. Wang, H.-Z. Lu, S.-Q. Shen, and F.-C. Zhang, Impurity effect on weak antilocalization in the topological insulator Bi_2Te_3, Phys. Rev. Lett. **106**, 166805 (2011).

[37] H.-Z. Lu, J. Shi, and S.-Q. Shen, Competition between weak localization and antilocalization in topological surface states, Phys. Rev. Lett. **107**, 076801 (2011).

[38] D. Hsieh, Y. Xia, D. Qian, L. Wray, J. H. Dil, F. Meier, J. Osterwalder, L. Patthey, J. G. Checkelsky, N. P. Ong, A. V. Fedorov, H. Lin, A. Bansil, D. Grauer, Y. S. Hor, R. J. Cava, and M. Z. Hasan, A tunable topological insulator in the spin helical Dirac transport regime, Nature (London) **460**, 1101 (2009).

[39] S. Souma, K. Kosaka, T. Sato, M. Komatsu, A. Takayama, T. Takahashi, M. Kriener, K. Segawa, and Y. Ando, Direct measurement of the out-of-plane spin texture in the Dirac-cone surface state of a topological insulator, Phys. Rev. Lett. **106**, 216803 (2011).

[40] L. Fu and C. L. Kane, Superconducting proximity effect and majorana fermions at the surface of a topological insulator, Phys. Rev. Lett. **100**, 096407 (2008).

[41] H.-H. Sun, K.-W. Zhang, L.-H. Hu, C. Li, G.-Y. Wang, H.-Y. Ma, Z.-A. Xu, C.-L. Gao, D.-D. Guan, Y.-Y. Li, C. Liu, D. Qian, Y. Zhou, L. Fu, S.-C. Li, F.-C. Zhang, and J.-F. Jia, Majorana zero mode detected with spin selective Andreev reflection in the vortex of a topological superconductor, Phys. Rev. Lett. **116**, 257003 (2016).

[42] D. Wang, L. Kong, P. Fan, H. Chen, S. Zhu, W. Liu, L. Cao, Y. Sun, S. Du, J. Schneeloch *et al.*, Evidence for Majorana bound states in an iron-based superconductor, Science **362**, 333 (2018).

[43] X.-L. Qi, T. L. Hughes, and S.-C. Zhang, Topological field theory of time-reversal invariant insulators, Phys. Rev. B **78**, 195424 (2008).

[44] A. M. Essin, J. E. Moore, and D. Vanderbilt, Magnetoelectric polarizability and axion electrodynamics in crystalline insulators, Phys. Rev. Lett. **102**, 146805 (2009).

[45] R. S. K. Mong, A. M. Essin, and J. E. Moore, Antiferromagnetic topological insulators, Phys. Rev. B **81**, 245209 (2010).

[46] M. Mogi, Y. Okamura, M. Kawamura, R. Yoshimi, K. Yasuda, A. Tsukazaki, K. S. Takahashi, T. Morimoto, N. Nagaosa, M. Kawasaki, Y. Takahashi, and Y. Tokura, Experimental signature of the parity anomaly in a semi-magnetic topological insulator, Nat. Phys. **18**, 390 (2022).

[47] H. Zhang, C.-X. Liu, X.-L. Qi, X. Dai, Z. Fang, and S.-C. Zhang, Topological insulators in Bi_2Se_3, Bi_2Te_3 and Sb_2Te_3 with a single Dirac cone on the surface, Nat. Phys. **5**, 438 (2009).

[48] C.-X. Liu, X.-L. Qi, H.-J. Zhang, X. Dai, Z. Fang, and S.-C. Zhang, Model Hamiltonian for topological insulators, Phys. Rev. B **82**, 045122 (2010).

[49] M. Kargarian, M. Randeria, and Y.-M. Lu, Are the surface Fermi arcs in Dirac semimetals topologically protected?, Proc. Natl. Acad. Sci. USA **113**, 8648 (2016).

[50] Z. Yan, Z. Wu, and W. Huang, Vortex end Majorana zero modes in superconducting Dirac and Weyl semimetals, Phys. Rev. Lett. **124**, 257001 (2020).

[51] S.-Y. Xu, C. Liu, S. K. Kushwaha, R. Sankar, J. W. Krizan, I. Belopolski, M. Neupane, G. Bian, N. Alidoust, T.-R. Chang *et al.*, Observation of Fermi arc surface states in a topological metal, Science **347**, 294 (2015).

[52] P. Zhang, Z. Wang, X. Wu, K. Yaji, Y. Ishida, Y. Kohama, G. Dai, Y. Sun, C. Bareille, K. Kuroda *et al.*, Multiple topological states in iron-based superconductors, Nat. Phys. **15**, 41 (2019).

[53] S. M. Young, S. Zaheer, J. C. Y. Teo, C. L. Kane, E. J. Mele, and A. M. Rappe, Dirac semimetal in three dimensions, Phys. Rev. Lett. **108**, 140405 (2012).

[54] Z. Wang, Y. Sun, X.-Q. Chen, C. Franchini, G. Xu, H. Weng, X. Dai, and Z. Fang, Dirac semimetal and topological phase transitions in A_3Bi (A = Na, K, Rb), Phys. Rev. B **85**, 195320 (2012).

[55] Z. Wang, H. Weng, Q. Wu, X. Dai, and Z. Fang, Three-dimensional Dirac semimetal and quantum transport in Cd_3As_2, Phys. Rev. B **88**, 125427 (2013).

[56] Z. K. Liu, B. Zhou, Y. Zhang, Z. J. Wang, H. M. Weng, D. Prabhakaran, S.-K. Mo, Z. X. Shen, Z. Fang, X. Dai *et al.*, Discovery of a three-dimensional topological Dirac semimetal, Na_3Bi, Science **343**, 864 (2014).

[57] Z. K. Liu, J. Jiang, B. Zhou, Z. J. Wang, Y. Zhang, H. M. Weng, D. Prabhakaran, S.-K. Mo, H. Peng, P. Dudin, T. Kim, M. Hoesch, Z. Fang, X. Dai, Z. X. Shen, D. L. Feng, Z. Hussain, and Y. L. Chen, A stable three-dimensional topological Dirac semimetal Cd_3As_2, Nat. Mater. **13**, 677 (2014).

[58] S. Borisenko, Q. Gibson, D. Evtushinsky, V. Zabolotnyy, B. Büchner, and R. J. Cava, Experimental realization of a three-dimensional Dirac semimetal, Phys. Rev. Lett. **113**, 027603 (2014).

[59] M. Neupane, S.-Y. Xu, R. Sankar, N. Alidoust, G. Bian, C. Liu, I. Belopolski, T.-R. Chang, H.-T. Jeng, H. Lin *et al.*, Observation of a three-dimensional topological Dirac semimetal phase in high-mobility Cd_3As_2, Nat. Commun. **5**, 3786 (2014).

[60] S. Qin, L. Hu, C. Le, J. Zeng, F.-chun Zhang, C. Fang, and J. Hu, Quasi-1d topological nodal vortex line phase in doped superconducting 3d Dirac semimetals, Phys. Rev. Lett. **123**, 027003 (2019).

[61] B.-J. Yang and N. Nagaosa, Classification of stable three-dimensional Dirac semimetals with nontrivial topology, Nat. Commun. **5**, 4898 (2014).

[62] M. Kargarian, Y.-M. Lu, and M. Randeria, Deformation and stability of surface states in Dirac semimetals, Phys. Rev. B **97**, 165129 (2018).

[63] C. Le, X. Wu, S. Qin, Y. Li, R. Thomale, F.-C. Zhang, and J. Huw, Dirac semimetal in β-CuI without surface Fermi arcs, Proc. Natl. Acad. Sci. USA **115**, 8311 (2018).

[64] T.-R. Qin, Z.-H.Chen, T.-X. Liu, F.-Y. Chen, H.-J. Duan, M.-X. Deng, and R.-Q. Wang, Quantum Hall effect in topological Dirac semimetals modulated by the Lifshitz transition of the Fermi arc surface states, arXiv:2309.08233.

[65] S. Kobayashi and M. Sato, Topological superconductivity in Dirac semimetals, Phys. Rev. Lett. **115**, 187001 (2015).

[66] M. Kheirkhah, Z.-Y. Zhuang, J. Maciejko, and Z. Yan, Surface Bogoliubov-Dirac cones and helical Majorana hinge modes in superconducting Dirac semimetals, Phys. Rev. B **105**, 014509 (2022).

[67] Z. Wu and Y. Wang, Nodal higher-order topological superconductivity from a $\mathcal{C}_4$-symmetric Dirac semimetal, Phys. Rev. B **106**, 214510 (2022).

[68] A. L. Szabó, R. Moessner, and B. Roy, Strain-engineered higher-order topological phases for spin-$\frac{3}{2}$ Luttinger fermions, Phys. Rev. B **101**, 121301(R) (2020).

[69] Y. Mo, X.-J. Wang, R. Yu, and Z. Yan, Boundary flat bands with topological spin textures protected by sub-chiral symmetry, arXiv:2307.01851.

[70] Z. Yan, F. Song, and Z. Wang, Majorana corner modes in a high-temperature platform, Phys. Rev. Lett. **121**, 096803 (2018).

[71] See Supplemental Material at http://link.aps.org/supplemental/10.1103/PhysRevB.109.L081401 for the derivation details of the low-energy surface Hamiltonians, spin textures, and Berry phases.

[72] Z. Yan and Z. Wang, Tunable Weyl points in periodically driven bodal line semimetals, Phys. Rev. Lett. **117**, 087402 (2016).

[73] Y. Cao, J. A. Waugh, X.-W. Zhang, J.-W. Luo, Q. Wang, T. J. Reber, S. K. Mo, Z. Xu, A. Yang, J. Schneeloch, G. D. Gu, M. Brahlek, N. Bansal, S. Oh, A. Zunger, and D. S. Dessau, Mapping the orbital wavefunction of the surface states in three-dimensional topological insulators, Nat. Phys. **9**, 499 (2013).

[74] S. R. Park, J. Han, C. Kim, Y. Y. Koh, C. Kim, H. Lee, H. J. Choi, J. H. Han, K. D. Lee, N. J. Hur, M. Arita, K. Shimada, H. Namatame, and M. Taniguchi, Chiral orbital-angular momentum in the surface states of Bi_2Se_3, Phys. Rev. Lett. **108**, 046805 (2012).

[75] H. Zhang, C.-X. Liu, and S.-C. Zhang, Spin-orbital texture in topological insulators, Phys. Rev. Lett. **111**, 066801 (2013).

[76] D. Xiao, M.-C. Chang, and Q. Niu, Berry phase effects on electronic properties, Rev. Mod. Phys. **82**, 1959 (2010).

[77] K. S. Novoselov, E. McCann, S. V. Morozov, V. I. Fal'ko, M. I. Katsnelson, U. Zeitler, D. Jiang, F. Schedin, and A. K. Geim, Unconventional quantum Hall effect and Berry's phase of 2π in bilayer graphene, Nat. Phys. **2**, 177 (2006).

[78] Y. L. Chen, J.-H. Chu, J. G. Analytis, Z. K. Liu, K. Igarashi, H.-H. Kuo, X. L. Qi, S. K. Mo, R. G. Moore, D. H. Lu, M. Hashimoto, T. Sasagawa, S. C. Zhang, I. R. Fisher, Z. Hussain, and Z. X. Shen, Massive Dirac fermion on the surface of a magnetically doped topological insulator, Science **329**, 659 (2010).

[79] Y. H. Wang, D. Hsieh, D. Pilon, L. Fu, D. R. Gardner, Y. S. Lee, and N. Gedik, Observation of a warped helical spin texture in Bi_2Se_3 from circular dichroism angle-resolved photoemission spectroscopy, Phys. Rev. Lett. **107**, 207602 (2011).

[80] B. Q. Lv, S. Muff, T. Qian, Z. D. Song, S. M. Nie, N. Xu, P. Richard, C. E. Matt, N. C. Plumb, L. X. Zhao, G. F. Chen, Z. Fang, X. Dai, J. H. Dil, J. Mesot, M. Shi, H. M. Weng, and H. Ding, Observation of Fermi-arc spin texture in TaAs, Phys. Rev. Lett. **115**, 217601 (2015).

[81] S.-Y. Xu, I. Belopolski, D. S. Sanchez, M. Neupane, G. Chang, K. Yaji, Z. Yuan, C. Zhang, K. Kuroda, G. Bian, C. Guo, H. Lu, T.-R. Chang, N. Alidoust, H. Zheng, C.-C. Lee, S.-M. Huang, C.-H. Hsu, H.-T. Jeng, A. Bansil *et al.*, Spin polarization and texture of the Fermi arcs in the Weyl fermion semimetal TaAs, Phys. Rev. Lett. **116**, 096801 (2016).

[82] M. Sakano, M. Hirayama, T. Takahashi, S. Akebi, M. Nakayama, K. Kuroda, K. Taguchi, T. Yoshikawa, K. Miyamoto, T. Okuda, K. Ono, H. Kumigashira, T. Ideue, Y. Iwasa, N. Mitsuishi, K. Ishizaka, S. Shin, T. Miyake, S. Murakami, T. Sasagawa *et al.*, Radial spin texture in elemental tellurium with chiral crystal structure, Phys. Rev. Lett. **124**, 136404 (2020).

[83] J. Dai, E. Frantzeskakis, N. Aryal, K.-W. Chen, F. Fortuna, J. E. Rault, P. Le Fèvre, L. Balicas, K. Miyamoto, T. Okuda, E. Manousakis, R. E. Baumbach, and A. F. Santander-Syro, Experimental observation and spin texture of Dirac node arcs in tetradymite topological metals, Phys. Rev. Lett. **126**, 196407 (2021).